

ANALYSIS OF MAGNETIC MEASUREMENTS OF SHORT MODEL QUADRUPOLES FOR THE LHC LOW- β INSERTIONS*

R. Bossert, J. Brandt, J. Carson, D. Chichili, H. Glass, J. DiMarco, S. Feher, T. Heger, Y. Huang, J. Kerby, M.J. Lamm, P.J. Limon, F. Nobrega, I. Novitski, D. Orris, J.P. Ozelis, T.J. Peterson, W. Robotham, G. Sabbi, P. Schlabach, J. Strait, C. Sylvester, M. Tartaglia, J. Tompkins, A.V. Zlobin, FNAL; S. Caspi, A.D. McInturff, R. Scanlan, LBNL

Abstract

The first two short models of the MQXB quadrupole magnets for the LHC interaction regions have been built and tested at Fermilab. In this paper we present the magnetic field measurement results and compare them with expectations based on as-built dimensional parameters and with a preliminary table of field quality requirements.

1 INTRODUCTION

The MQXB design is based on a 2-layer, $\cos(2\theta)$ coil operating in superfluid helium at 1.9 K [1]. A magnet model program aimed at validating and optimizing this design is under way. The first short model (HGQ01) was tested in the Fermilab Vertical Magnet Test Facility in February 1998. The second short model (HGQ02) was tested in June 1998. In this paper, magnetic measurements of the two models are discussed and compared with calculations [2].

A rectangular coordinate system is defined with the z axis at the center of the magnet aperture and pointing from the return end towards the lead end, the x axis horizontal and pointing to the right of an observer who faces the magnet from the lead end, the y axis vertical and pointing upwards. The field is represented in terms of harmonic coefficients defined by the power series expansion

$$B_y + iB_x = B_2 10^{-4} \sum_{n=1}^{\infty} (b_n + ia_n) \left(\frac{x + iy}{r_0} \right)^{n-1}$$

where B_x and B_y are the field components, B_2 is the quadrupole field, b_n and a_n are the $2n$ -pole coefficients. The reference radius r_0 is 17 mm [3].

In order to provide a common reference for the discussion of field quality issues from the viewpoint of magnet fabrication, machine performance and IR systems layout, a preliminary field quality specification for MQXB magnets has been established [4]. For each harmonic component, the expected values of the mean, uncertainty in mean and standard deviation are listed in Table 1. These values will be used as reference for the discussion of field quality measurements of the first two model magnets.

Table 1: MQXB reference harmonics [4].

n	$\langle b_n \rangle$	$d(b_n)$	$\sigma(b_n)$	$\langle a_n \rangle$	$d(a_n)$	$\sigma(a_n)$
Straight section						
3	0.0	0.34	0.85	0.0	0.34	0.85
4	0.0	0.26	0.87	0.0	0.26	0.87
5	0.0	0.20	0.34	0.0	0.20	0.34
6	0.0	0.17	0.25	0.0	0.17	0.25
7	0.0	0.14	0.11	0.0	0.14	0.11
8	0.0	0.10	0.07	0.0	0.10	0.07
9	0.0	0.08	0.07	0.0	0.08	0.07
10	0.0	0.06	0.03	0.0	0.06	0.03
Lead end (magnetic length 0.41 m)						
2	0.0	0.0	0.0	38	0.0	0.0
6	5.5	0.0	0.0	0.2	0.0	0.0
10	-0.2	0.0	0.0	-0.1	0.0	0.0
Return end (magnetic length 0.33 m)						
6	1.2	0.0	0.0	0.0	0.0	0.0
10	-0.3	0.0	0.0	0.0	0.0	0.0

2 MEASUREMENT SYSTEM

Cold magnetic measurements of HGQ01 were performed using a vertical drive, rotating coil system obtained from the SSCL. The rotating coil has 5 windings on a machined ceramic probe form: tangential, 2 dipole bucking, and 2 quadrupole bucking windings. This probe has nominal diameter 25.4 mm and length 25 cm. A new probe optimized for 70 mm aperture magnets was commissioned for the HGQ02 test. It has 40.6 mm nominal diameter and length 91 cm. The winding design is similar to that of the SSCL probe. Coil winding voltages are read out using 5 HP3458 DVMs. An additional DVM is used to monitor magnet current. The DVMs are triggered simultaneously by an angular encoder on the probe shaft, synchronizing measurements of field and current. Feed down of the quadrupole signal to the dipole is used to center the probe in the magnet.

3 FIELD QUALITY ANALYSIS

Figure 1 shows the dependence of the magnet transfer function (G/I) on current. Due to iron saturation, a 2% decrease is observed in the current range 1-10 kA. The nominal current for MQXB is 0.8 kA at injection, 11.1 kA in collision.

* Work supported by the U.S. Department of Energy

Between the first and the second model, a 0.2% difference in the low-current transfer function is observed, which may be related to probe calibration. Good agreement is found between measured values and design calculations (a 98% packing factor for the yoke laminations is assumed).

Figure 2 shows the dependence of the normal dodecapole on current in HGQ01. At low ramp rates, the mean of up and down ramps reflects the contributions of iron saturation and conductor displacement under Lorentz forces, while the difference between mean values and up-down ramps is due to persistent currents in the superconducting coil. The observed change in the mean b_6 is very small over the entire current range and in good agreement with design calculations, as shown in Fig. 3. The persistent current b_6 at injection is less than 1 unit. No significant dependence of b_{10} on current was observed.

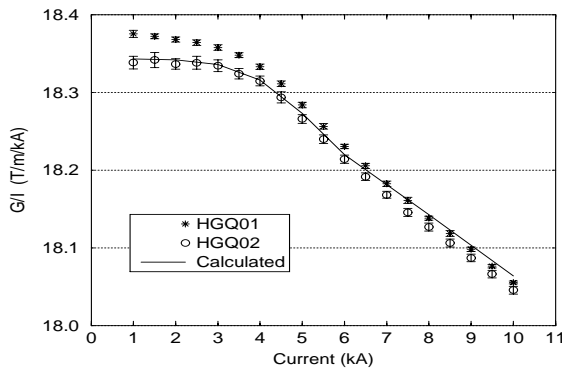


Figure 1: Transfer function vs. current.

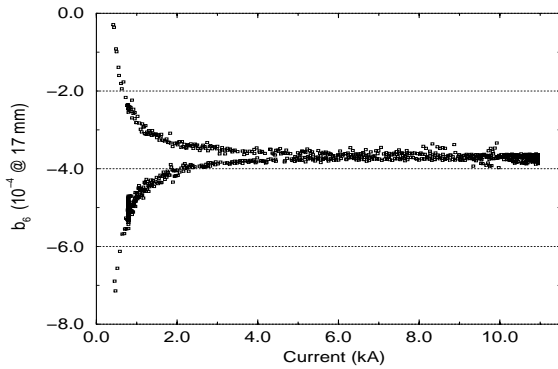


Figure 2: Normal dodecapole vs current.

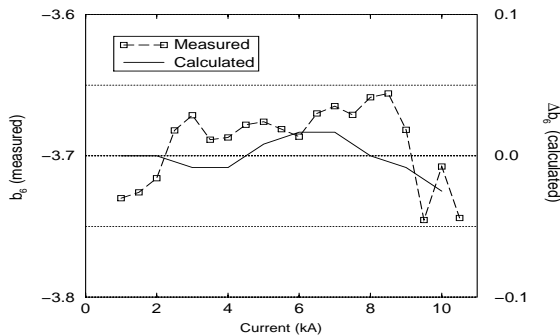


Figure 3: Saturation and Lorentz force effect on b_6 .

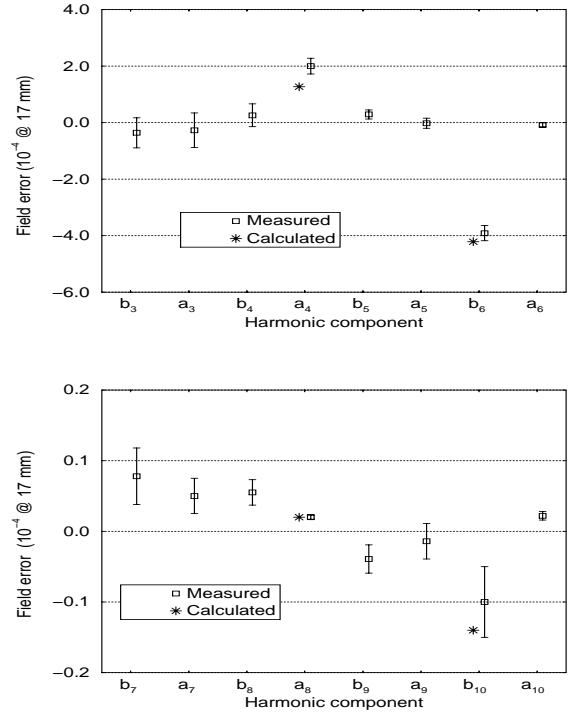


Figure 4: HGQ01 body harmonics.

Table 2: Average central harmonics at 6 kA.

n	Normal (b_n)		Skew (a_n)	
	HGQ01	HGQ02	HGQ01	HGQ02
3	-0.36	-0.74	-0.27	0.52
4	0.26	0.14	2.00	0.51
5	0.29	0.11	-0.02	-0.22
6	-3.91	-1.46	-0.08	0.01
7	0.08	-0.02	0.05	-0.01
8	0.06	0.01	0.02	0.02
9	-0.04	0.01	-0.01	-0.02
10	-0.10	-0.10	0.02	0.01

Figure 4 shows the average field harmonics and corresponding standard deviations measured in a longitudinal scan of the HGQ01 straight section in 25 cm steps, at 4.2 K, 6 kA. Due to thick coil shims (up to 450 μm) needed to obtain the required prestress, the b_6 and b_{10} components are large with respect to specifications. However, their values are in good agreement with calculations based on as-built parameters. Due to a difference in size of 80 μm between the inner coils in quadrant 1 and 3 and those in quadrant 2 and 4, and the corresponding adjustments of shim thickness, non zero values are expected also for the harmonics components a_4 and a_8 . Good agreement is found between the calculated and measured a_8 , while some discrepancy is observed for the skew octupole a_4 .

In HGQ02, a reduction of the coil shim thickness by a factor of 2 was obtained by adjusting the cable insulation scheme and the coil curing procedure, with a corresponding

improvement in the field quality. A comparison between the body harmonics for the two models is shown in Table 2. Further improvements of the field quality will be obtained by optimizing the coil fabrication procedure. In HGQ03, the coil shim thickness is reduced by another factor of 2 with respect to HGQ02. Small residual systematics will be corrected by adjustments of the cable or wedge dimensions.

Magnetic measurements of the HGQ01 lead end have been performed at a sequence of positions along the z axis, in steps of 2 cm. Due to the presence of a longitudinal field component, and to the dependence of the transfer function on the longitudinal position, the local end field is best described in terms of field integrals over the probe length, at the probe radius. A comparison between calculated and measured normal dodecapole is shown in Fig. 5. The design values have been corrected to take into account the effect of coil shims, which extend into the end regions. The total integrated multipoles for the lead end can be calculated from the field integrals at the probe radius and scaled to the 17 mm reference radius (Table 3). The comparison between calculation and measurement indicates that the uncertainty in design harmonics is within 0.5 units for the normal and skew dodecapole, 0.1 units for the normal and skew 20-pole.

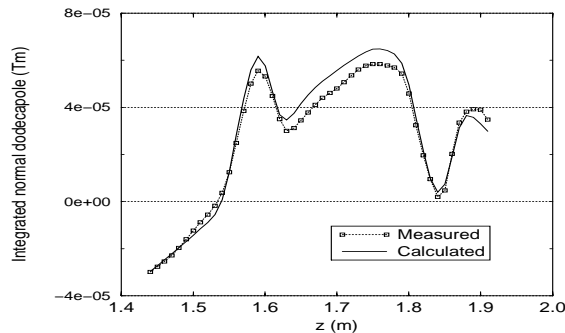


Figure 5: Normal dodecapole in HGQ01 lead end.

Table 3: Comparison of integrated multipoles at the reference radius in the interval [1.31,2.03] m.

Parameter	Measured	Calculated
L_m (m)	0.41	0.41
b_6	2.9	3.1
a_6	0.1	0.5
b_{10}	-0.3	-0.3
a_{10}	-0.1	-0.1

Table 4: Magnetic shim correction ($I=10$ kA).

Component	Measured	Calculated
Δb_3	0	-0.1
Δa_3	-2.6	-2.8
Δb_4	+0.5	+0.5
Δa_4	+0.2	+0.3

The HGQ design incorporates magnetic shims for correction of low-order non-allowed geometric harmonics. Between the first and second thermal cycle, one of the shims was extracted from HGQ01. The resulting change in low-order harmonics is shown in Table 4. While a good tuning range and decoupling between the effect of different shims is obtained for the normal and skew sextupole, the effect decreases rapidly for increasing multipole orders. No significant change is observed for $n \geq 5$. Due to iron saturation, the magnetic shim effect is strongly current-dependent. A given correction at nominal gradient results in an overcompensation of about a factor of 2 at injection (Fig. 6).

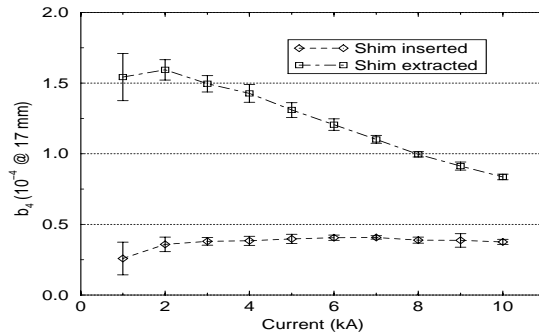


Figure 6: Magnetic shim effect on b_4 .

4 CONCLUSIONS

Magnetic measurements of the first two HGQ models confirm design calculations for geometric harmonics, magnetization and Lorentz force effects, harmonic correction with geometric/magnetic shims, and end field. In HGQ01, due to coil shims needed to obtain the required prestress and compensate for differences in coil size, large field errors are present. By adjusting the cable insulation scheme and coil curing procedure, significant improvements were obtained in HGQ02. A further reduction of the field errors is expected in HGQ03. With respect to the MQXB reference harmonics listed in Table 1, experimental results confirm that the goal of zero systematic value for all straight section harmonics can be met within the specified uncertainty. The systematic errors which are present in the current end design are expected to be substantially reduced after final optimization [5]. For the random errors, both the total integrated (non-allowed) harmonics in the two models and local measurements carried out with a short probe along the length of HGQ01 show values comparable to the standard deviations listed in the reference table.

5 REFERENCES

- [1] R. Bossert, et al., Proc. MT-15 Conf., October 1997.
- [2] G. Sabbi, et al., Proc. MT-15 Conf., October 1997.
- [3] L. Walckiers, P. Lefevre, LHC-MTA/LW, April 1998.
- [4] W. Chou, et al., Fermilab Pub-97/378, November 1997.
- [5] G. Sabbi, Fermilab TD-98-037, May 1998.